A&A 444, 213–220 (2005)
DOI: 10.1051/0004-6361:20053711

Astronomy & Astrophysics

Doppler tomography of the asynchronous polar BY Camelopardalis⋆

R. Schwarz[1], A. D. Schwope[1], A. Staude[1], and R. A. Remillard[2]

[1] Astrophysikalsches Institut Potsdam, An der Sternwarte 16, 14482 Potsdam, Germany
e-mail: rschwarz@aip.de
[2] Center for Space Research, Massachusetts Institute of Technology, Cambridge, MA 02139, USA

Received 28 June 2005 / Accepted 1 August 2005

ABSTRACT

We present phase-resolved, high-resolution (1.3 Å) spectroscopy of the brightest near-synchronous polar BY Cam taken on two different occasions in 1998 and 1999. The first tomographic study of such a system reveals line emission spread out over a large velocity range forming a crescent at negative v_y velocities in the Doppler maps. In contrast to the majority of synchronous AM Her systems there is only weak indication for the presence of a focused accretion stream. These two facts suggest that the majority of the matter is accreted via an extended curtain. Location and extent of the structure in the Doppler maps can be reproduced with a simple curtain model raised over a wide (∼180°) range in azimuth implying that the ballistic stream stretches to a point far behind the white dwarf. In order to reach such small magnetospheric radii mass accretion rates a factor of 10 to 20 in excess of that normally seen in polars would be required. In addition to the curtain emission, the Balmer lines show a narrow emission line component likely originating from the heated side of the secondary star. Its velocity amplitude of 190 km s^{-1} together with an illumination model of the secondary star suggests a rather heavy white dwarf of $M_1 \geq 0.8\ M_\odot$ and an inclination larger than $i \geq 40°$. Timings of this feature in the present and historical data unequivocally determine the orbital period and have been used to establish a high-precision, long-term ephemeris.

Key words. accretion: accretion disks – stars: binaries: close – stars: novae, cataclysmic variables – stars: magnetic fields

1. Introduction

BY Cam is the brightest ($V \sim 14^{\rm m}$) of the four known asynchronous polars (or AM Herculis stars) and the second magnetic cataclysmic variable (CV) after V1500 Cyg (Nova 1975) to be identified as such. In these hybrids between the synchronised, high-field AM Herculis stars (or polars) and the rapidly rotating DQ Herculis systems (or intermediate polars, IPs), the accreting white dwarf is out of synchronisation with the orbital period by a few percent. Contrary to the majority of intermediate polars accretion is not disk-fed (Hellier 2002), but is believed to occur along a confined accretion stream. During a beat cycle set by $P_{\rm spin}$ and $P_{\rm orb}$ the orientation between the magnetic field axis and the ballistic stream continually changes and infalling matter should couple onto different field lines and possibly switch to the energetically favoured pole. These objects are therefore key targets for the understanding of the physics of the mass transfer in the case of a varying magnetic field geometry.

Despite heroic efforts in the last two decades progress on the details of the accretion process in these systems has been slow. Early follow-up observations after the identification with the HEAO1 scanning modulation collimator experiment (Remillard et al. 1986) revealed properties common to the class of AM Herculis binaries: variations at optical and X-ray wavelengths with a tentative spin period of 200 min, strong circular polarisation (mostly of positive sign), optical low states down to $V \geq 17^{\rm m}$ as measured from Harvard plates and the detection of cyclotron humps consistent with a magnetic field strength of 40.8 MG (Cropper et al. 1989) or 28 MG (Schwope 1991).

Subsequent photometric and polarimetric monitoring (Mason et al. 1989; Piirola et al. 1994) revealed marked phases of strong (+10%) positive circular polarisation accompanied by a drop of the total intensity modelled in the context of two-pole accretion. However, strong nightly changes in the light curves dissimilar to that of synchronised magnetic CVs prohibited an unequivocal determination of a spin ephemeris using the timings of the polarisation features: the two tentative spin periods 199.33 min (Mason et al. 1989) and 199.849 min (Piirola et al. 1994) differ by multiples of the claimed errors and were not confirmed independently later.

Secure confirmation of the asynchronism was achieved by the detection of a longer orbital period at 201.899 min based on the variations of a narrow component in the Hα emission line (Silber et al. 1992). This tentative orbital period was

⋆ Based on observations collected at the German-Spanish Astronomical Centre, Calar Alto, operated by the MPI für Astronomie, Heidelberg, jointly with the Spanish National Commission for Astronomy.

later refined to 201.323 min by Sauter (1992), using a similar technique but better data. Surprisingly, the orbital period, rather than the spin period, was also detected in the flux and velocity modulation of the N v line λ1240 Å from a two-weeks IUE monitoring by Zucker et al. (1995).

In an attempt to clarify the confusing situation Mouchet et al. (1997) critically reviewed previous period determinations and presented own spectroscopic data which also showed a narrow component in the Balmer lines. To complicate this difficult matter even further, their value for $P_{\rm orb}$ = 202.901 min is in clear disagreement with the other estimates. Their re-analysis of the Zucker et al. data dismissed the N v line velocities as a tracer of the orbital period, but yielded a shorter period and a phase jump, which they attributed to gas near the surface of the white dwarf.

An intensive photometric campaign spanning several months of near continuous monitoring (Silber et al. 1997; Mason et al. 1998) led to the detection of a previously unrecognised shorter period of 197.439 min dominating the signals anticipated for $P_{\rm spin}$ and $P_{\rm orb}$. Taking the different pieces of evidence together, Silber et al. (1997) concluded that this shorter period must be the $2\omega - \Omega$ sideband frequency, thus indirectly validating $P_{\rm spin}$ and $P_{\rm orb}$ at or close to the values found by Mason et al. (1989) and Sauter (1992). If this interpretation is correct, BY Cam has a beat period of ∼14 days, and the presence of the $2\omega - \Omega$ sideband frequency would be an indirect evidence for pole switching as predicted from the theoretical power spectra (Wynn & King 1992).

Doppler tomography, the reconstruction of a two-dimensional velocity map from a set of phase-resolved emission or absorption line profiles (Marsh & Horne 1988; Marsh 2001) has widely been used for detailed imaging of structures in cataclysmic binaries, like the emission from the stream/disk impact region (Skidmore et al. 2000), spiral shocks in accretion disks of outbursting dwarf novae (Steeghs et al. 1997), or possible slingshot prominences settled within in the binary system (Steeghs et al. 1996). The method is particularly suited for the case of strongly magnetic, synchronised AM Her systems and possibly the near-synchronised polars, since there the accretion flow is fixed within the co-rotating binary frame – a prerequisite of the inversion process. At present there are about a dozen high quality Doppler maps of AM Her systems published typically showing some or all of the three following characteristic features:

(a) A sharp component at $v_x = 0$ due to the ubiquitous emission from a quasi-chromosphere at the heated frontside of the secondary star. Data of highest resolution and sufficient signal-to-noise can resolve the Roche lobe in Doppler coordinates (Schwarz et al. 2002) and reveal asymmetric illumination of the secondary (Schwope et al. 1997; Watson et al. 2003).
(b) Emission from the stream leaving the secondary star through the L_1-point, seen as a cometary tail parallel to the v_x axis. Good examples where this horizontal stream is the dominant emitting source are the maps of the eclipsing polars HU Aqr (high state, Schwope et al. 1997) and V1309 Ori (Staude et al. 2001). The exact location in the tomogram should follow that of a ballistic trajectory (Lubow & Shu 1975) and is determined by the systems mass ratio only. There are, however, some cases like AM Her (Schwarz et al. 2002) or QQ Vul (Schwope et al. 2000) where such purely hydro-dynamical flow cannot account for the observed trajectory, possibly indicating the influence of the magnetic field of the secondary star. Furthermore, the width of the ballistic streams tangential to the infall velocity is much wider then predicted (Heerlein et al. 1999).
(c) The infalling material will encounter the rapidly increasing field of the primary and eventually couple onto the field lines at a point r_μ where magnetic pressure equals the ram pressure of the stream. Magnetically controlled streams have been observed in several systems (HU Aqr, low state: Schwope et al. 1998; UZ For: Schwope et al. 1999; QQ Vul: Schwope et al. 2000; AR UMa: Schmidt et al. 1999) which have in common rather high magnetic fields ($B > 30$ MG). The trajectory is mainly set by the field geometry and observations are roughly in agreement with dipolar fields connecting to the accretion region on the white dwarf. In all these cases the ballistic streams are truncated at velocities < 500 km s^{-1} indicating coupling at large distances from the white dwarf.

In this paper we present the first study which applies Doppler tomography to an asynchronous polar.

2. Observations

BY Cam was the target of two runs at the 3.5 m telescope at Calar Alto, Spain in November 1998 and December 1999 with the ultimate goal to obtain Doppler tomograms around the beat cycle. Weather conditions permitted observations on only two nights, November 19, 1998 and December 19, 1999, of a total of 10 allocated nights. The double-beam TWIN spectrograph used was set up in the red arm with the grating T06 for both runs, which disperses light at 0.54 Å/pixel and covered the range from 6400 to 7450 Å. For the blue arm different gratings T01 (2. order; 0.39 Å/pixel) and T05 (0.54 Å/pixel) were employed in 1998 and 1999. These were centred roughly at 4500 Å and covered a range of 780 and 1000 Å. Together with the 1.5″ slit used, these configurations yielded resolutions of 1.35 Å (red, blue 1998) and 1.0 Å (blue 1999) *FWHM* as measured with arc-lamp spectra. After standard wavelength and flux calibration the absolute flux of the spectra was recalibrated using star #9 from Henden & Honeycutt (1995) simultaneously kept in the slit. At the time of the observations BY Cam was in a bright state and varied between $B = 15\overset{\rm m}{.}8$–$15\overset{\rm m}{.}2$ comparable with previous high-state measurements (Piirola et al. 1994). The blue average spectrum displayed in Fig. 1 is rich in hydrogen, helium and metal emission lines. The lines are extremely broad and extend up to velocities of HWZI ∼ 3500 km s^{-1}, best seen in the blueshifted wings of the Balmer lines. The line-flux of BY Cam increased by 45% during the observation in December 1999, while the continuum flux brightened by 30% only. Also the flux ratio of He II λ 4686 to Hβ increased from 1.1 to 1.2 indicating a real change of the ionisation conditions.

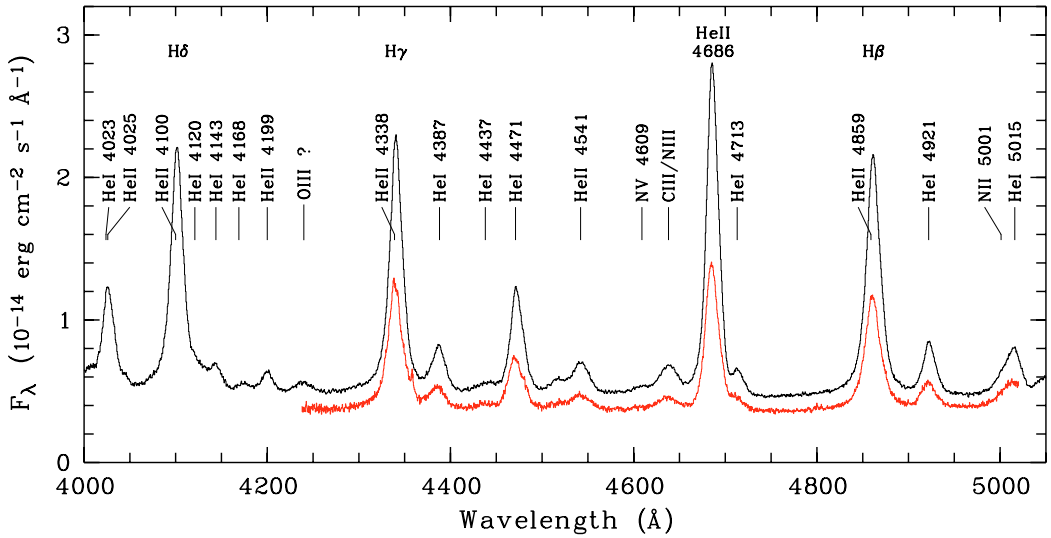

Fig. 1. Flux-calibrated average spectra of BY Cam obtained on November 19, 1998 (*bottom*) and December 19, 1999 (*top*).

3. Results

3.1. Trailed spectra

In Fig. 2 we show the phase-averaged trailed spectra of the two major emission lines Hβ and He II λ4686. The other Balmer lines and He I λ4471 behaved very similar to Hβ and are not discussed further. The data were folded according to the new orbital ephemeris determined in this paper and given in Sect. 3.2. Both lines have a distinct appearance which significantly changed from one occasion to the other. The major difference between Hβ and He II λ4686 is a narrow (*FWHM*~ 120 km s^{-1}) emission line component (NEL), which is only seen in the Balmer lines moving sinusoidally with an amplitude of ~200 km s^{-1}. This component is possibly the same as that previously noted by Mason et al. (1989), Silber et al. (1992) and Mouchet et al. (1997), and likely emerges from the heated side of the companion star. In line with this interpretation the narrow component exhibits strong orbital photometric variability expected due to the changing visibility of the front side. During the phase interval 0.75–0.25 the NEL is completely invisible indicating a rather high binary inclination >45°.

The weakness or even absence of the NEL in the He II λ4686 line is quite remarkable, since for most synchronised AM Herculis stars the emission from the secondary star is of comparable strength in He II λ4686 and the Balmer lines. As photoionisation is the only excitation mechanism at the surface of the companion and the presence of He II λ4686 requires photons with energies >54 eV, effective shielding of the secondary from soft X-ray's must be operating in BY Cam.

The underlying broad components from the accretion flow are much less structured in BY Cam compared to the trailed spectra of synchronised polars. Nonetheless we can identify a fast moving, high velocity component in the 1998 data, changing from maximum positive velocity of 800 km s^{-1} at phase 0.1 to maximum negative velocity −800 km s^{-1} at phase 0.4, and vice versa between phase 0.6 and 0.9. It resembles somewhat the appearance of the ballistic accretion stream in the trailed spectra of HU Aqr (Schwope et al. 1997). The fading of this component around phases 0 and 0.5 can be explained by the large velocity dispersion as one looks parallel along the stream at these phases.

In addition to that stream emission, there is another distinct, broad component shifted by about 0.5 units in phase. It is seen as blueshifted emission with −800 km s^{-1} around phase zero and half an orbit later at maximum redshift of 800 km s^{-1}. Such a phasing directly implies that we see gas moving towards the secondary star, and not away from it as expected for the ballistic and magnetic trajectories normally observed for polars. While the Balmer lines are strongly blurred due to optical depth effects, the He II λ4686 line reveals subtle substructure, with two phases of maximum redshift at ϕ = 0.4 and ϕ = 0.65, but high-velocity emission missing at phase 0.55.

During the later 1999 observation the trailed spectra are less structured and show strong intrinsic variability on time scales of a few minutes which make the identification of separate line components difficult. The ballistic stream component previously seen is only marginally detectable in the light of the He II λ4686 line, while the aforementioned peculiar emission redward of the NEL is clearly evident but shifted to an earlier phase around ϕ ~ 0.4. Similar to the 1998 data although with a smaller amplitude there is blueshifted emission at ϕ = 0.0. Quite remarkably the line profiles peak at, or near zero velocity for most phases, forming a quasi-stationary low amplitude component. Given the complicated profiles and the strong blending of the line components, especially in the case of the 1999 data set, we did not attempt a Gaussian deconvolution but proceed with a tomographic analysis of the spectra.

3.2. Doppler tomograms: emission from the secondary and orbital ephemeris

Doppler tomograms of the Hβ and He II λ4686 lines for the two occasions are displayed in Fig. 3. They have been computed from continuum subtracted spectra using the MEM-based implementation of Spruit (1998). The velocity resolution of the maps have been set to 13 km s^{-1} and the used value of the regularisation parameter α = 0.001 and a smearing kernel

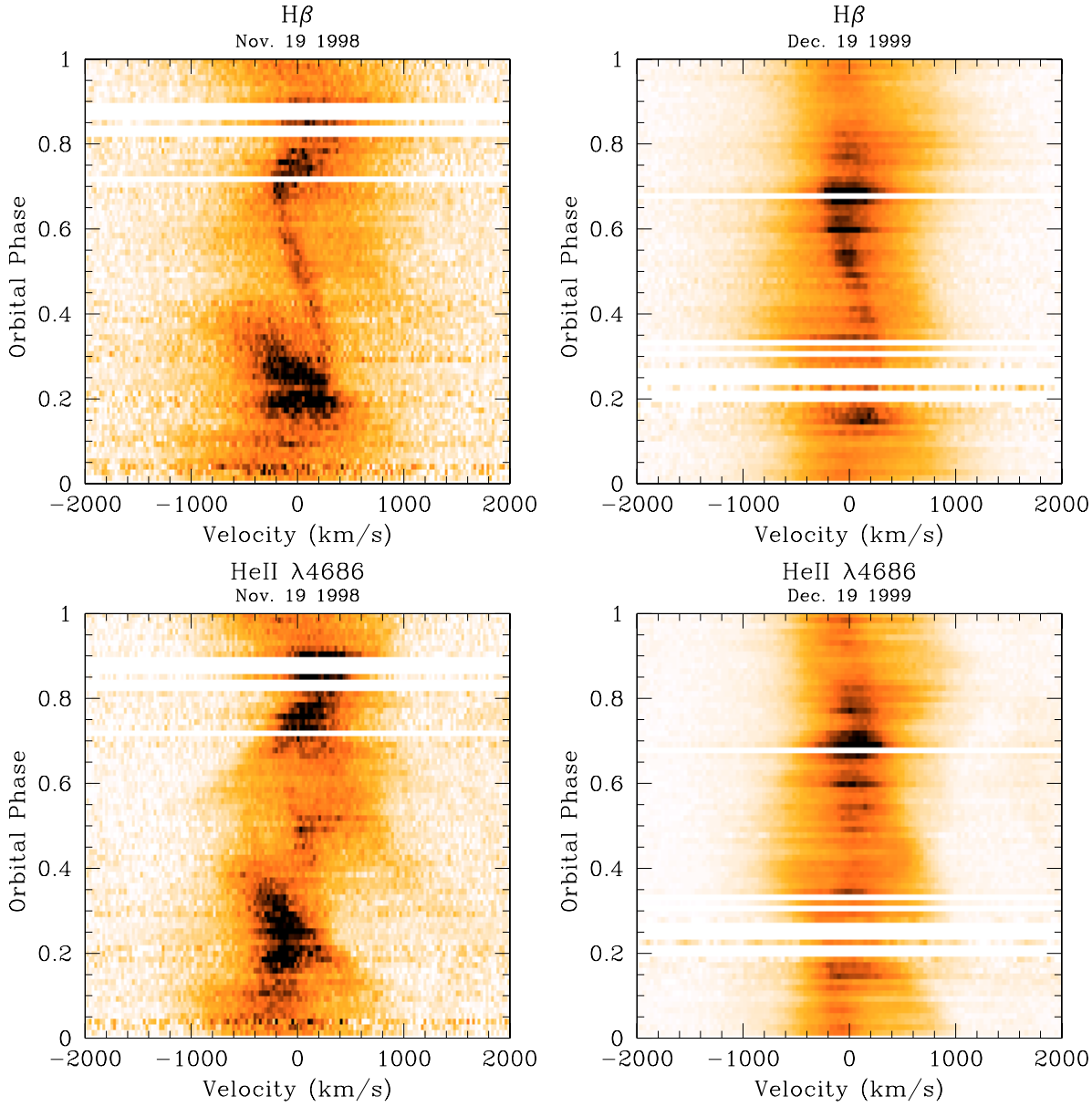

Fig. 2. Trailed spectrograms of the Hβ and He II λ4686 emission lines. Phase have been computed with new orbital ephemeris derived in this paper.

of 5 pixels ensured a good balance between preserved information and noise in the map.

Another important input parameter is a correct systemic velocity, which has not been determined beforehand, e.g. by a sine-fit to the NEL. A possible way is to use the appearance of the secondary star, which can be clearly seen in the Hβ maps as a sharp point-like feature. We iteratively computed a series of test maps spanning a wide range of possible γ-values. For maps with wrong γ-values the emission from the secondary star is significantly elongated, while for the adapted value of zero velocity shift the emission is restricted to the expected location of the secondary star. After heliocentric correction this value yields a systemic velocity of 10 km s^{-1} in close agreement with previous estimates (Mason et al. 1989).

The projected velocity amplitude $K_2' = (v_x^2 + v_y^2)^{-1/2}$ of the secondary star emission can be used for a dynamical mass estimate of the white dwarf. The values determined from Gaussian fits to the NEL in the two data sets are 192 and 188 km s^{-1} with a formal error of $\pm$4 km s^{-1}. These velocities correspond to the photocentre of the line emission at the frontside and are clearly smaller than the true velocity of centre of mass K_2. In order to correct this effect we applied an illumination model of the secondary star. This model is described in Beuermann & Thomas (1990) and calculates white dwarf mass $M_{\rm wd}$ and inclination i for a given velocity of an uniformly illuminated Roche lobe. We explicitly suppose a secondary's mass M_2 according to a ZAMS mass-radius relationship (in our case Caillault & Patterson 1990). We further assume that line emission is confined to the frontside only. The more sophisticated approach of Roche tomography (Rutten & Dhillon 1994; Watson et al. 2003), which would allow for an arbitrary brightness distribution appears not feasible given the rather noisy and

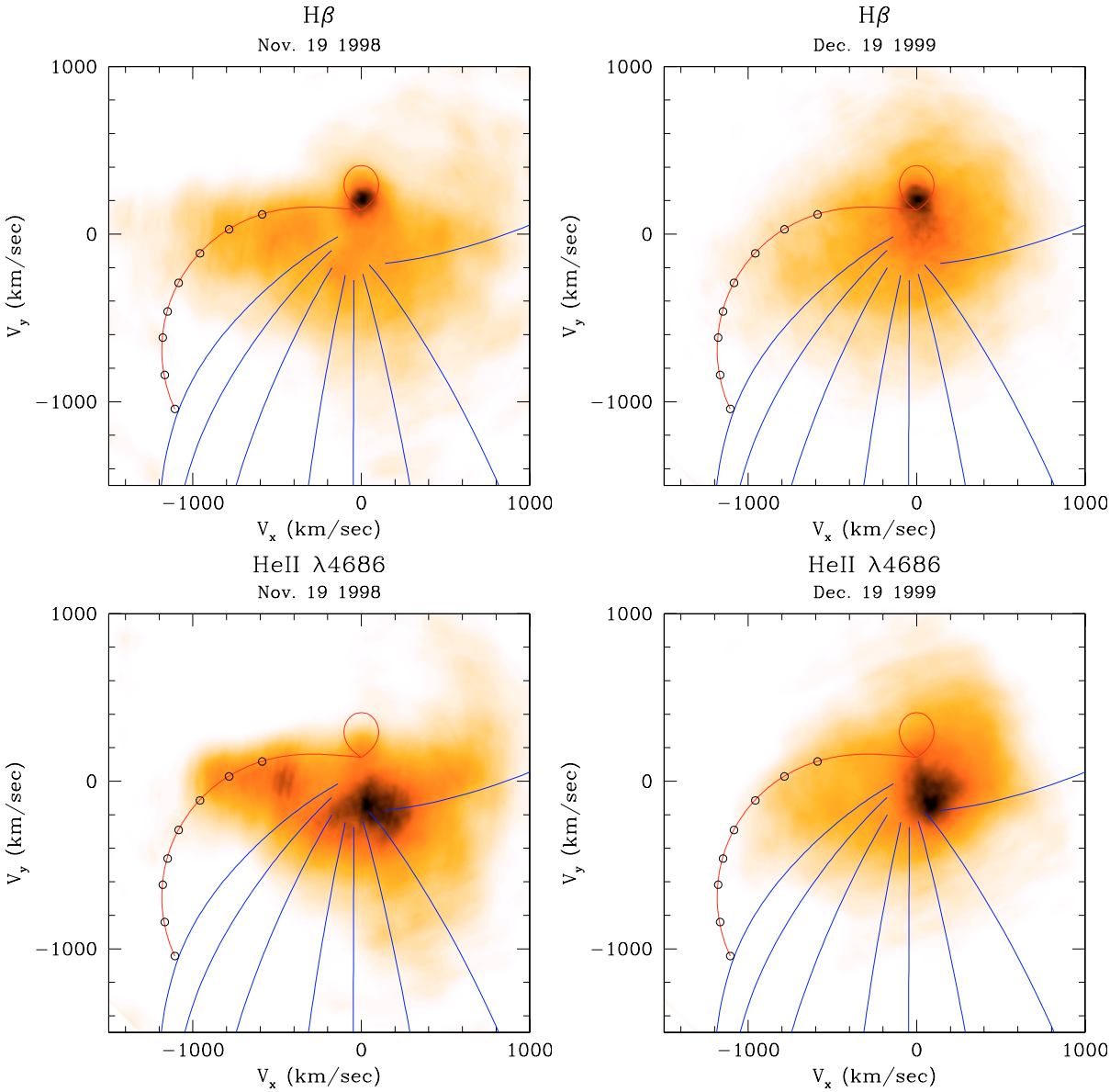

Fig. 3. Doppler maps of BY Cam computed from Hβ and He II λ 4686 emission lines observed in 1998 and 1999. Overlayed are the locations of the secondary star, a ballistic trajectory (both red), and a set of magnetic trajectories representing an extended curtain (blue). Small circles mark the positions where those trajectories are leaving the ballistic stream.

highly blended NEL component and the lack of complementary absorption line information in BY Cam. Our computed parameter pairs ($M_{\rm wd}$, i) for $K_2' = 190\,{\rm km\,s^{-1}}$ do impose relative tight lower limits for the white dwarf ($\geq$0.8 $M_\odot$) mass and binary inclination ($i \geq 40°$), set by the maximum possible inclination of $i \leq 74°$and the Chandrandsekar mass limit.

The location of the secondary star within the binary frame can be obtained from the phasing $\Delta\phi = \arctan v_x/v_y$ of the secondary star emission in the Doppler map. In this way we determined timings of inferior conjunction from test maps using a preliminary orbital period which should be sufficiently close to the true value to prevent artefacts from wrong folding. In order to enlarge the baseline for the determination of the orbital period we also included older spectroscopic measurements. These comprise of 336 spectra of the Hα emission line obtained on five nights between November, 20 and 27 1991 at the 1.3 m McGrawHill telescope of the Michigan-Dartmouth-MIT (MDM) observatory and were used in the study of Sauter (1992). Doppler maps computed from these data, although much noisier, still show a narrow emission spot from the secondary star and timings were extracted in a similar manner. In addition, fifteen radial-velocity measurements of the narrow component in Hβ obtained on March 10 and 12, 1991 with the SAO 6 m telescope as presented in Fig. 5 of Mouchet et al. (1997) were fitted with a sine function yielding a further timing of the inferior conjunction.

For a total of 8 blue-to-red zero crossings given in Table 1 we then applied a search algorithm, that for each trial period computes the standard deviations $\sum$(O−C)^2 from a linear relationship. In the periodogram (Fig. 4) showing the inverse of $\sum$(O−C)^2 a maximum is found at a best period of 201.24 min, accompanied by a few alias periods whose standard deviations

Table 1. Heliocentric timings of the zero-velocity crossing of the NEL.

Telescope	Date	$T_{\rm NEL}$ (HJD 2 400 000+)	O–C (10^{-4} d)	$\Delta T_{\rm NEL}$	Cycle
SAO 6 m	10/12-Mar.-91	48 326.4104	39	29	−20 114
MDM 1.3 m	20-Nov.-91	48 580.7555	−12	17	−18 294
MDM 1.3 m	21-Nov.-91	48 581.7377	27	17	−18 287
MDM 1.3 m	22-Nov.-91	48 582.7154	21	17	−18 280
MDM 1.3 m	23-Nov.-91	48 583.6844	−71	17	−18 273
MDM 1.3 m	27-Nov.-91	48 587.7436	−7	17	−18 244
CA 3.5 m	19-Nov.-98	51 137.3949	−2	7	0
CA 3.5 m	19-Dec.-99	51 532.4770	6	7	2827

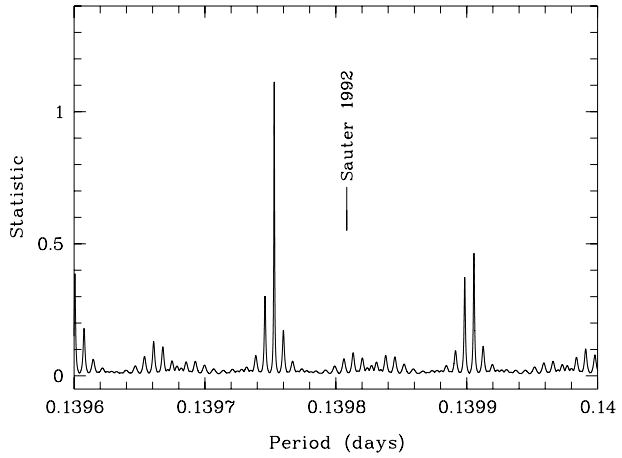

Fig. 4. Periodogram using the χ^2 method applied to the timings of blue-red zero-crossings of the narrow component of the Balmer lines. The likely period of 0.139791 days (201.199 min) and other spectroscopic measurements of the orbital period are indicated.

with respect to linear relationship exceed that of the best value by a factor of 3 or more. The preferred value of $P_{\rm orb}$ is within the error range quoted for the period of Sauter (1992), but does exclude the measurements of Silber et al. (1992) and Mouchet et al. (1997). A linear regression to the timings of inferior conjunction gives

$$T_{\rm NEL}({\rm HJD}) = 2\,451\,137.3952(36) + E \times 0.13975284(14)$$

where the number in brackets denote the uncertainties in the last digits. Most of the residuals with respect to that ephemeris are within the formal errors (see Table 1), but there are a few outliers which might be explained by other systematic error sources like wrong γ-values or noise within the Doppler maps.

3.3. Doppler tomograms: accretion curtain emission

Beside emission from the secondary star the two tomograms taken in 1998 and 1999 are characterised by a peculiar crescent-shape structure seen in the two lower quadrants spanning a wide range of v_x velocities. Such a feature has not yet been observed in any of the synchronised polars. It is, however present in the spin-cycle tomograms of several intermediate polars Hellier (1999), where it is interpreted as the signature of an accretion curtain. The arc in the tomogram subtends over 180° at the origin, implying that the putative accretion curtain covers this range of azimuth also in binary coordinates. The location in the tomogram suggests that the curtain is raised all along the ballistic stream from the L_1-point to a stagnation region far beyond the white dwarf. In the tomogram taken in 1999 the accretion arc is rotated about the origin by ∼45° extending now to positive v_y of ∼500 km s^{-1}. Thus, at that occasion the material must have travelled around the white dwarf even further, before being finally captured.

Contrary to the Balmer lines where the curtain emission is smoothly distributed, the He II λ4686 line peaks in a broad structure around $(v_x, v_y) \sim (0, -200)$ km s^{-1}. The brightness in that area is enhanced by factor of 2 compared to the adjacent curtain emission. Such low velocities may correspond to material that has just been decelerated after being captured by the magnetic field.

In the 1998 tomogram there is some indication for a ballistic stream moving parallel to the v_x-axis up to velocities of $v_x \sim -1000$ km s^{-1}, where it abruptly becomes invisible. The stream appears to be rather broad in v_y-direction and is brightest slightly below the path of a ballistic trajectory, possibly due to blending with emission from the curtain. For the 1999 observation the ballistic stream is either not present, or extends to lower velocities only and can therefore not discriminated from the curtain.

In order to explore possible conditions which may lead to the formation of an accretion curtain we set up a binary model which computes single-particle trajectories threadened onto a dipolar magnetic field line. Stream coupling in this model is determined by the balance of magnetic pressure $B^2/8\pi$ and ram pressure ρv^2. The basic binary parameters (i, M_1, M_2) were fixed at values (62°, 0.9 $M_\odot$, 0.29 $M_\odot$) consistent with the dynamical mass estimate made in the previous section. For the magnetic field we assumed a magnetic moment $\mu = 3.3 \times 10^{33}$ G cm^3 implied by the measurement of Schwope (1991), while the stream densities were derived from the mass accretion rate assuming a fixed stream cross-section of 0.75×10^{18} cm^2 given by the formulae in Meyer & Meyer-Hofmeister (1983). We then computed trajectories in binary and Doppler coordinates for various dipole orientations and mass accretion rates. Co-latitudes smaller than $\beta < 20°$ are preferred, since they predict low velocities for the material just coupled to the field and which are required

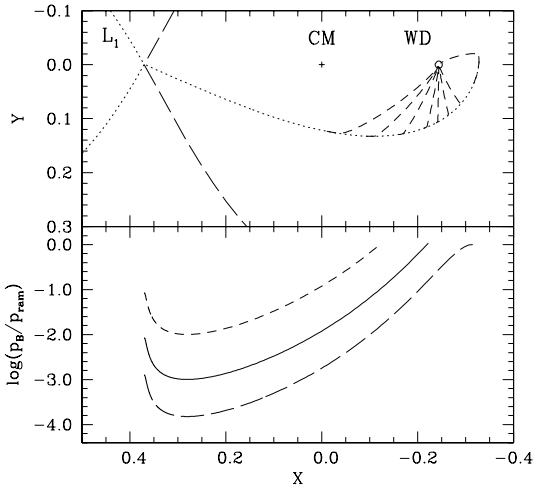

Fig. 5. (*Upper panel*) Geometry of the suspected accretion curtain projected onto the orbital plane. Assumed are system parameters and a dipole orientation as outlined in Sect. 3.2. Indicated are the Roche lobes of both stars, the L_1-point, the white dwarf and the centre of mass. The curtain is represented by 8 magnetic trajectories, also shown in velocity coordinates (Fig. 3). Coupling occurs over a range of azimuth from $\psi_{\rm thread} = 35°$ to 175°. (*Lower panel*) The ratio of magnetic and ram pressure along the stream, for three exemplary mass accretion rates ($\dot{M} = 1 \times 10^{-11}, 1 \times 10^{-10}, 6.6 \times 10^{-10}\ M_\odot\ {\rm yr}^{-1}$) needed to reach the range of coupling radii implied by the extent of the accretion curtain.

to explain the peak of emission at $(v_x, v_y) \sim (0, -200)\ {\rm km\,s^{-1}}$. We note however, that this constraint implicitly follows from our treatment of the energy dissipation in the coupling region which assumes the conversion of the velocities components parallel to the field lines. As the physics of the coupling process is largely unconstrained by either theory or observation, complete dissipation of the kinetic energy is a viable alternative, which will result in low velocity emission for any given co-latitude. With our choice of a small β, the value for the azimuth ψ does not have a strong influence on the appearance of the magnetic trajectories. We will therefore assume in the following a dipole axis at an azimuth of $\psi = 88°$ and a co-latitude of $\beta = 14°$.

In Figs. 3 and 5 we show model trajectories based on this geometry, but for a range of mass accretion rates, which partly reproduce the structures observed. In order to account for the large extent of the curtain, coupling must occur over a wide range along the ballistic stream. In particular, a fraction of the material must pass behind the white dwarf and become captured at an azimuth as large as $\psi_{\rm thread} = 160$–$180°$, in order to explain the emission from material moving towards the secondary star seen in the lower right of the tomograms. The mass accretion rates required to reach those magnetospheric radii range from $\dot{M} = 0.5 \times 10^{-11}\ M_\odot\ {\rm yr}^{-1}$ for early coupling (near an azimuth $\psi_{\rm thread} \sim 30°$) up to $\dot{M} = 6.6 \times 10^{-10}\ M_\odot\ {\rm yr}^{-1}$ in the case of very late threading.

While this rather simple model provides a good match with the observed tomograms its fair to mention also a few discrepancies, which may require further discussion:

(i) The ballistic stream tentatively detected in the map from 1998 does extend only to velocities of $(v_x, v_y) \sim (-1000, 0)\ {\rm km\,s^{-1}}$. In case of an elongated curtain, one would expect to see an associated ballistic stream at very high velocities (lower left-quadrant Fig. 3) which is not detected. One possible explanation would be intrinsically low line emission from this part of the ballistic stream due to the physical conditions of the gas. Beside shielding of high energy photons by inter-binary material, the most obvious parameters are the rapidly decreasing density ($\propto v_{\rm ff}^{-1}$) and the stronger irradiation as the material approaches the white dwarf.

(ii) The magnetic curtain is visible only up to moderate velocities ($v < 1000\ {\rm km\,s^{-1}}$), much lower than the free-falling velocity to which the material will be accelerated. In principle, the high velocity part of the curtain will undergo similar density and irradiation conditions as suggested above for the ballistic stream. In addition, the curtain material is lifted out of the orbital plane implying non-negligible z-velocities. This effect does depend on the orbital inclination, and might be of importance in a system with an intermediate range of inclinations like BY Cam. Possible ring-like artefacts introduced into Doppler maps are nicely illustrated by Staude et al. (2004). In general, this effect reduces the observed line-of-sight velocity and smears out the emission, which both can influce the missing high velocity emission.

(iii) For the 1999 observation the curtain is rotated counter-clockwise towards the upper left quadrant of the tomogram, indicating that material can reach an azimuth larger than 180°. This rotation may indicate a real change of the accretion geometry, but can presently not be represented with our coupling model. Particles reaching those velocities have such high kinetic energy that they actually never couple onto the magnetic field and form a curtain in the tomogram.

In summary, we conclude that most of the differences between the curtain model and observed tomogram are due to a lack of an appropriate prescription of the ionisation conditions and the coupling mechanism.

4. Discussion

The first Doppler tomograms taken of an asynchronous polar are clearly dominated by emission which probably originates from an accretion curtain. The ballistic accretion stream, ubiquitous in the tomograms of synchronous polars, was rather dim in 1998, and not detectable during the 1999 observation. If true, the large extent of the accretion curtain in BY Cam implies that part of the free-falling material does deeply enter into magnetosphere white dwarf without being coupled to the field. Our model calculations predict that accretion rates in the order of $\dot{M} = 7 \times 10^{-10}\ M_\odot\ {\rm yr}^{-1}$ are required for such a deep penetration. This number is a factor of two higher than the empirical value expected for a CV at this orbital period (Patterson 1984). A different comparison is provided by the relative increase of the accretion rate by a factor of 10 to 20 needed to move the stagnation region from azimuth of $\psi \sim 30°$ normally seen in polars to a value of 180°. Unfortunately no estimate of the accretion rate in BY Cam is available due to its unknown

distance. The fact that this system is a likely post-nova and no spectroscopic signatures of the secondary star in this bright, long-period system have yet been found, do indeed argue a large distance and a high accretion rate.

Other than synchronised AM Her stars which have very similar dipole orientations pointing towards the secondary star (Cropper 1988), the accretion geometry of asynchronous polars constantly changes during the beat cycle. At times a disadvantageous dipole orientation (e.g. perpendicular to the infalling ballistic stream) may foster the formation of an accretion curtain. One would therefore suggest that the appearance of the curtain should be a function of the beat phase. The putative rotation of the curtain of ∼45° from one occasion to the other may be an indication of this. Further observations, with a denser coverage of the entire beat cycle, should provide a stringent test of this possibility. Alternatively, this effect may reflect an increased accretion rate consistent with the increased brightness for the 1999 observation.

Accretion curtains are known to exist in synchronous systems too, but their detection have to rely on indirect indicators, such as X-ray absorption or extended impact regions on the white dwarf. For the best documented case HU Aqr, where both methods are applicable (Schwope et al. 2001, 2003), it could be shown that only a small fraction (∼10%) of the material is accreted this way. This observation is in rather good agreement with calculations for gas stripping along the ballistic stream (Heerlein et al. 1999). Similar calculations, for the likely situation of BY Cam e.g. higher accretion rates and different field geometries should clarify if such extended accretion curtain is the natural consequence of stream stripping.

Extended curtains may be the characteristic mode of accretion for all asynchronous AM Herculis stars. The large size of ∼1500 km of the X-ray emitting region in V1432 Aql recently measured from RXTE eclipse light curves (Mukai et al. 2003), provides clear, though indirect evidence for such structure in a second system.

Finally, two decades after its discovery the orbital period of BY Cam has been firmly established using the spectroscopic signature of the heated front side of the secondary star. The ephemeris is accurate enough to link the huge amount of optical and X-ray data already available. This will open a new way for a qualitative understanding of the yet unknown accretion geometry and its changes along the beat cycle.

Acknowledgements. R.S. was and is supported by the Deutsches Zentrum für Luft- und Raumfahrt (DLR) GmbH under contracts No. FKZ 50 OR 9706 8, 50 OR 0206 and 50 OR 0404. We would like to thank Martine Mouchet for kindly providing their SAO radial velocity measurements.

References

Beuermann, K., & Thomas, H.-C. 1990, A&A, 230, 326
Caillault, J., & Patterson, J. 1990, AJ, 100, 825
Cropper, M. 1988, MNRAS, 231, 597
Cropper, M., Mason, K. O., Allington-Smith, J. R., et al. 1989, MNRAS, 236, 29
Heerlein, C., Horne, K., & Schwope, A. D. 1999, MNRAS, 304, 145
Hellier, C. 1999, ApJ, 519, 324
Hellier, C. 2002, in The Physics of Cataclysmic Variables and Related Objects, ASP Conf. Ser., 261, 92
Henden, A. A., & Honeycutt, R. K. 1995, PASP, 107, 324
Lubow, S. H., & Shu, F. H. 1975, ApJ, 198, 383
Marsh, T. R. 2001, in Astrotomography, Indirect Imaging Methods in Observational Astronomy, 1
Marsh, T. R., & Horne, K. 1988, MNRAS, 235, 269
Mason, P. A., Liebert, J., & Schmidt, G. D. 1989, ApJ, 346, 941
Mason, P. A., Ramsay, G., Andronov, I., et al. 1998, MNRAS, 295, 511
Meyer, F., & Meyer-Hofmeister, E. 1983, A&A, 121, 29
Mouchet, M., Bonnet-Bidaud, J. M., Somov, N. N., & Somova, T. A. 1997, A&A, 324, 109
Mukai, K., Hellier, C., Madejski, G., Patterson, J., & Skillman, D. R. 2003, ApJ, 597, 479
Patterson, J. 1984, ApJS, 54, 443
Piirola, V., Coyne, G. V., Takalo, S. J., et al. 1994, A&A, 283, 163
Remillard, R. A., Bradt, H. V., McClintock, J. E., et al. 1986, ApJ, 302, L11
Rutten, R. G. M., & Dhillon, V. S. 1994, A&A, 288, 773
Sauter, L. 1992, Ph.D. Thesis, MIT
Schmidt, G. D., Hoard, D. W., Szkody, P., et al. 1999, ApJ, 525, 407
Schwarz, R., Hedelt, P., Rau, A., Staude, A., & Schwope, A. D. 2002, in The Physics of Cataclysmic Variables and Related Objects, ASP Conf. Ser., 261, 167
Schwope, A. D. 1991, Ph.D. Thesis, Technical University Berlin
Schwope, A. D., Mantel, K.-H., & Horne, K. 1997, A&A, 319, 894
Schwope, A. D., Beuermann, K., Buckley, D. A. H., et al. 1998, in Wild Stars in the Old West, ASP Conf. Ser., 137, 44
Schwope, A. D., Schwarz, R., Staude, A., et al. 1999, in Annapolis Workshop on Magnetic Cataclysmic Variables, ASP Conf. Ser., 157, 71
Schwope, A. D., Catalán, M. S., Beuermann, K., et al. 2000, MNRAS, 313, 533
Schwope, A. D., Schwarz, R., Sirk, M., & Howell, S. B. 2001, A&A, 375, 419
Schwope, A. D., Thomas, H.-C., Mante, K.-H., Haefner, R., & Staude, A. 2003, A&A, 402, 201
Silber, A., Bradt, H. V., Ishida, M., Ohashi, T., & Remillard, R. A. 1992, ApJ, 389, 704
Silber, A. D., Szkody, P., Hoard, D. W., et al. 1997, MNRAS, 290, 25
Skidmore, W., Mason, E., Howell, S. B., et al. 2000, MNRAS, 318, 429
Spruit, H. C. 1998 [arXiv:astro-ph/9806141]
Staude, A., Schwope, A. D., Hedelt, P., Rau, A., & Schwarz, R. 2004, in Magnetic Cataclysmic Variables, IAU 190, ASP Conf. Ser., 315, 251
Staude, A., Schwope, A. D., & Schwarz, R. 2001, A&A, 374, 588
Steeghs, D., Harlaftis, E. T., & Horne, K. 1997, MNRAS, 290, L28
Steeghs, D., Horne, K., Marsh, T. R., & Donati, J. F. 1996, MNRAS, 281, 626
Watson, C. A., Dhillon, V. S., Rutten, R. G. M., & Schwope, A. D. 2003, MNRAS, 341, 129
Wynn, G. A. & King, A. R. 1992, MNRAS, 255, 83
Zucker, D. B., Raymond, J. C., Silber, A., et al. 1995, ApJ, 449, 310